A comparative DFT study on antioxidative activity of 3- and 4-phenylcoumarins: an aspect of structure, electronics, mechanism, kinetics, and metal chelate relations

Article *in* Structural Chemistry · October 2023

DOI: 10.1007/s11224-023-02183-3

CITATIONS

0

3 authors, including:

Dau Duc

Vinh University

36 PUBLICATIONS **114** CITATIONS

SEE PROFILE

Son Ninh The

Vietnam Academy of Science and Technology

107 PUBLICATIONS **707** CITATIONS

SEE PROFILE

Structural Chemistry
https://doi.org/10.1007/s11224-023-02183-3

RESEARCH

A comparative DFT study on antioxidative activity of 3- and 4-phenylcoumarins: an aspect of structure, electronics, mechanism, kinetics, and metal chelate relations

Phan Thi Thuy[1] · Dau Xuan Duc[1] · Ninh The Son[2]

Received: 15 March 2023 / Accepted: 2 May 2023

Abstract
The current study aims to compare antioxidative activity of 3-phenylcoumarin 7-dihydroxy-3-(3′,4′-dihydroxyphenyl) chromenone (1) and 4-phenylcoumarin 6,7-dihydroxy-4-(3′,4′-dihydroxyphenyl)chromenone (2) by a DFT (density functional theory) calculation. Thermodynamic and kinetic actions of two studied coumarins 1–2 were considered at the M06-2X/6–311++G(d,p), in which their antiradical activity is due to hydroxy bond breaking. The HAT mechanism is essential for two compounds in gas and benzene, but the SPL-ET mechanism is a principal route in methanol and water. Hydroxy groups at C-6 and C-4′ of both two compounds, on the one hand, have induced the lowest BDE values of 76.8–79.6 kcal/mol in gas and benzene, and the lowest PA values of 37.4–40.8 kcal/mol in methanol and water, on the other hand, are the best groups the kinetic reactions with $HOO^{\bullet}$ and $^{\bullet}NO_2$ radicals. 1–6-OH shows the best acidity with the lowest pK_a value of 8.65. Phenyl hydroxyl groups of compound 1 have chelations to Fe^{2+}, to form the most stable complex with the lowest IE value of −189.6 kcal/mol, and the highest MIA value of 284.7 kcal/mol. In general, the antioxidative activity of 3-phenylcoumarin 1 is better than that of 4-phenylcoumarin 2.

Keywords Coumarin · Hydroxy group · Antioxidant · Density functional theory · Comparison

Introduction

With a wide range of great pharmacological values and low toxic levels, numerous natural products, especially phenolic compounds like flavonoids and coumarins, are utilized as medicines and food preservatives in many communities [1]. A significant area of study is the discovery of novel pharmacologically active chemicals from natural sources and the synthesis of their more potent analogs.

Coumarins (2*H*-chromen-2-ones) are a subclass of benzopyrone derivatives [2]. They are compounds formed from plants naturally or synthetically, and exhibited a wide range of biological activities, such as anti-bacteria, anticancer, antivirus, anti-hypertension, anti-inflammation, anti-arrhythmia, anti-osteoporosis, and anti-asthma, especially in terms of antioxidative activity [1, 2]. Coumarins can affect the formation and quenching of ROS (reactive oxygen species), thereby indicating tissue-protective antioxidative features [3]. It is also recognized that coumarin derivatives would help to monitor the location, amount, and retention time of RNS (reactive nitrogen species) in living organisms [4].

7-Dihydroxy-3-(3′,4′-dihydroxyphenyl)chromenone (**1**) was classified in the group of 3-phenylcoumarins, whereas 6,7-dihydroxy-4-(3′,4′-dihydroxyphenyl)chromenone (**2**) has been fallen into a class of 4-phenylcoumarin derivatives. In 2016, they were successfully synthesized by Perkin and Pechmann reactions [5]. Significantly, these two compounds might have therapeutic potentials for treatments of diseases characterized by free radical overproduction since their IC_{50} values of 0.049–0.055 mM were lower than that of the positive control trolox (IC_{50} 0.093 mM) in DPPH (2,2-diphenyl-1-picrylhydrazyl) radical quenching assay [5].

In the pharmaceutical sector, the computational chemistry has been developed into a discipline that actively supports several facets of drug design, such as target selection, lead

✉ Ninh The Son
ntson@ich.vast.vn

[1] Faculty of Chemistry, College of Education, Vinh University, 182 Le Duan, Vinh City, Nghean, Vietnam

[2] Institute of Chemistry, Vietnam Academy of Science and Technology (VAST), 18 Hoang Quoc Viet, Caugiay, Hanoi, Vietnam

Published online: 10 May 2023

identification, and lead optimization. While the organizational innovations are the key for the successes, the methodological advancements have been essential to the calculated progresses. In particular, the helpful role is the interactions between computational and medicinal chemistry, as well as the incorporation of computational chemistry across the entire drug discovery process. The DFT (density functional theory) is recognized as a principal approach to the electronic-structural theory problems, whereas the functionals, such as BLYP, B3LYP, PDE, PBE0, and M06-2X, are widely used [6–8]. For instance, Karadjova et al. have successfully explained the structural and energy changes occurring during dissociation of O–H bonds when considering radical scavenging actions of a series of synthetic 3-phenylcoumarins by the DFT method [9].

To the best of our knowledge, no report describes a comparative computational study on antioxidative potentials of compounds **1–2**. By means of DFT approach, the aim of the current research is to highlight the effects of structural-electronic properties, and their potential antioxidative mechanism, acidic evaluation, and metal chelation.

Theoretical methodology

It is recommended that the functional M06-2X is the most reliable in the case of deprotonated prediction [10]. Therefore, this functional was used to carry out the DFT computational processes [11–13]. At the M06-2X/6–311++G(d,p) level, geometrical processes for a general molecule M-OH and its derivatives $M–O^{\bullet}$, $M\text{-}OH^{\bullet+}$, and $M–O^{-}$ have been thoroughly optimized [11]. All the ground states without imaginary frequency were confirmed by vibrational frequency calculation. To consider solvent effects, the IEF-PMC (integral equation formalism of the polarizable continuum method) was generally used during geometrically optimized steps [11–13].

In general, three known antioxidative mechanisms, including hydrogen atom transfer (HAT), single electron transfer-proton transfer (SET-PT), and sequential proton loss-electron transfer (SPL-ET), can be assigned to compounds **1–2** (Fig. 1) [14].

The HAT is characterized by the BDE (bond dissociation energy). The IP (ionization potential) and the PDE (proton dissociation enthalpy) are responsible for the first and second steps of the SET-PT, respectively. Meanwhile, the PA (proton affinity) and the ETE (electron transfer enthalpy) are used to explain the first and second steps of the SPL-ET, respectively.

$$\mathrm{BDE} = \mathrm{H(M - O^{\bullet})} + \mathrm{H(H^{\bullet})} - \mathrm{H(M - OH)} \quad (1)$$

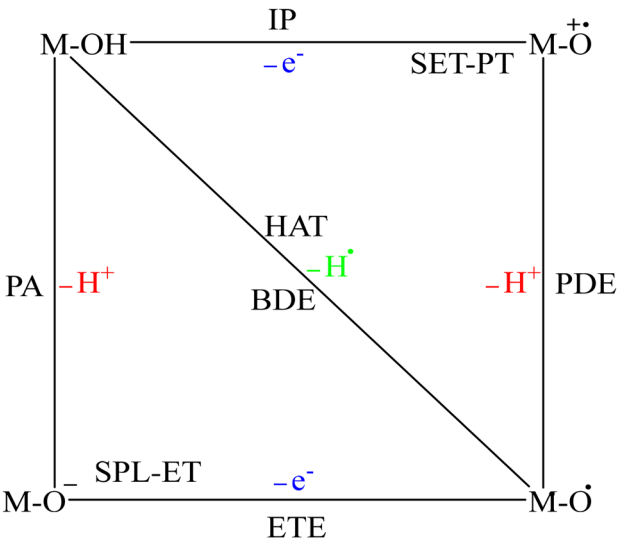

Fig. 1 The plausible antioxidative mechanisms for compounds **1–2**

$$\mathrm{IP} = \mathrm{H\left(M - O^{+\bullet}\right)} + \mathrm{H(e^{-})} - \mathrm{H(M - OH)} \quad (2)$$

$$\mathrm{PDE} = \mathrm{H(M - O^{\bullet})} + \mathrm{H\left(H^{+}\right)} - \mathrm{H(M - O^{\bullet+})} \quad (3)$$

$$\mathrm{PA} = \mathrm{H(M - O^{-})} + \mathrm{H\left(H^{+}\right)} - \mathrm{H(M - O)} \quad (4)$$

$$\mathrm{ETE} = \mathrm{H(M - O^{\bullet})} + \mathrm{H(e^{-})} - \mathrm{H(M - O^{-})} \quad (5)$$

The enthalpy H of e^{-} and H^{+} were extracted from similar reports [15].

The TST (transition state theory) was used to consider the kinetic actions of compounds **1–2** [11, 12]. The rate constant K has a relation to $\Delta G^{\#}$ (Gibbs free energy of activation) by Eq. (6).

$$K(\mathrm{T}) = \kappa \frac{\mathrm{T.k_B}}{\mathrm{h}} \mathrm{e}^{\frac{-\Delta G^{\#}}{\mathrm{RT}}} \quad (6)$$

where κ is the Wigner coefficient, and h and k_B stand for the Plank and Boltzmann constants, respectively.

Results and discussion

Structural analysis

It should be noted that the behavior of aromatic hydroxy groups in phenolic compounds is widely acknowledged as the main cause of antioxidative activity [16]. Structural optimization of two coumarins **1–2** was performed at the M06-2X/6–311++G(d,p) level, by which the ground structure of each compound resembled in all studied mediums gas,

benzene, methanol, and water (Fig. 2). In each compound, the π-electrons are found to be distributed in both coumarin nucleus (ring AC) and phenyl ring (ring B). However, the coplanarity between coumarin nucleus and phenyl ring is lost with dihedral angle θ (C_2-C_3-$C_{1'}$-$C_{6'}$) of 39.49°–44.62° in compound **1** and θ(C_3-C_4-$C_{1'}$-$C_{6'}$) of 52.34°–53.59° in compound **2** (Table S1). Hydrogen bonds between *ortho* hydroxy groups in compound **1** reach 2.111–2.118 Å, while two pairs of *ortho* hydroxy groups in compound **2** induce hydrogen bonds with the distance of 2.134–2.139 Å. The distance between hydrogen and oxygen in each hydroxy group fluctuates from 0.960 to 0.976 Å. However, hydroxy distance is observed to be slightly increased by 0.001–0.002 Å when converted gas into solvents. Therefore, it is desirable to use solvents for reducing hydroxyl bond cleavages.

To elucidate the relative position between coumarin nucleus and phenyl ring, the dependent curve of the optimized energies on dihedral angel θ was set up (Fig. 3). The step of scanning was carried out with a change of 10° from −180° to 180° (Table S2). As can be seen from compound **1**, a global conformer locates at ± 40°, whereas a local conformer is found to peak at ± 170° with the relative energy Δ*E* of 0.72 kcal/mol. Compound **1** is also accompanied by the presence of three energy barriers at ± 180°, ± 90°, and 0° with the Δ*E* values of 3.44, 2.97, and 2.37 kcal/mol, respectively. Also in Fig. 3 and Table S2, the scanning curve of compound **2** has given rise to a global conformer at ± 50°, two local conformers at −120° (Δ*E* = 0.52 kcal/mol) and 130° (Δ*E* = 0.64 kcal/mol), and three barriers at ± 180° (Δ*E* = 11.40 kcal/mol), ± 90° (Δ*E* = 1.22 kcal/mol), and 0 (Δ*E* = 9.23 kcal/mol).

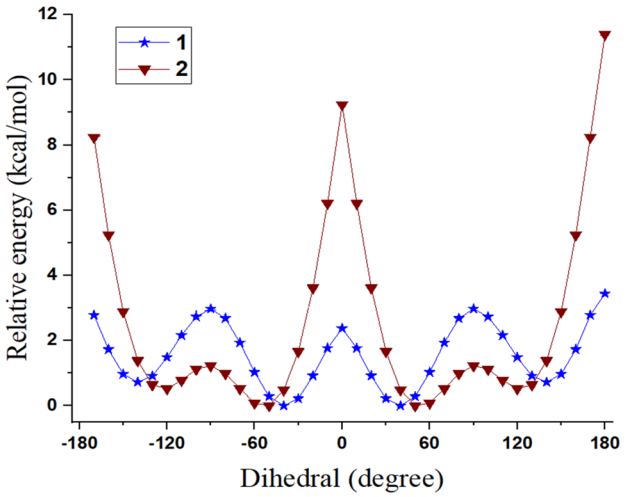

Fig. 3 Potential energy curves versus the dihedral angles θ_2 (C_2-C_3-$C_{1'}$-$C_{6'}$)/(C_3-C_4-$C_{1'}$-C_6)

Fig. 2 General structures of compounds **1**–**2** with atom numbering and their optimized forms at the M06-2X/6–311++G(d,p) level

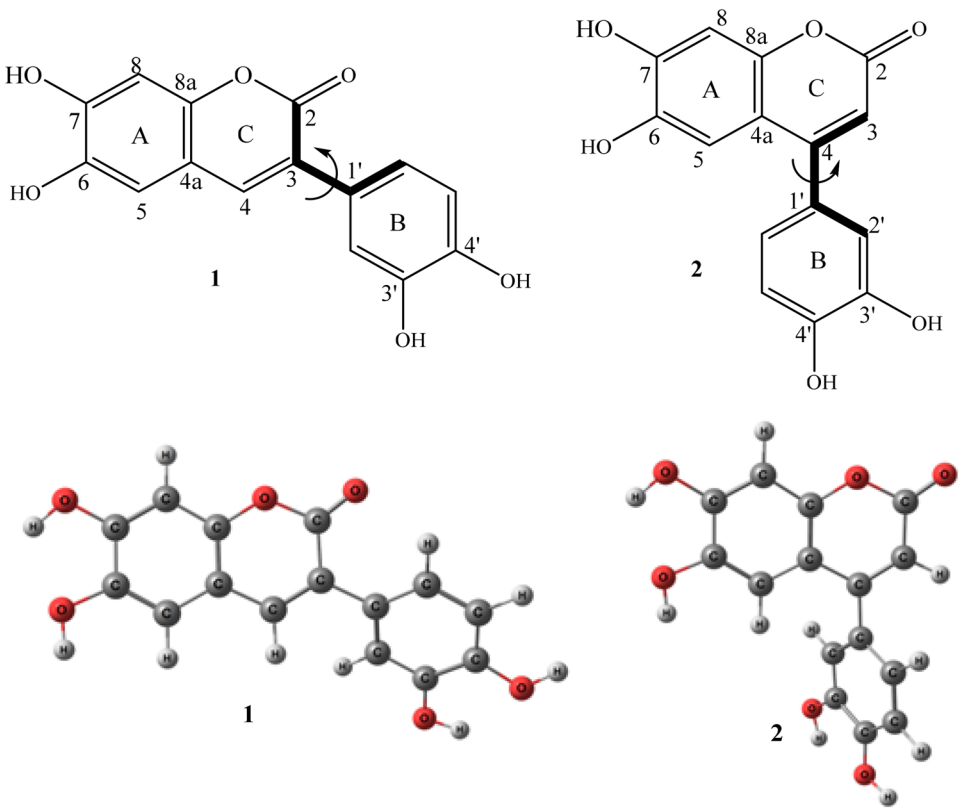

Frontier molecular orbital (FMO) and spin density

The neutral HOMO (highest occupied molecular orbital) and LUMO (lowest unoccupied molecular orbital) density plots can be used to understand how electron delocalization. For Fig. 4, the electrons have been observed to delocalize in whole parts of molecules **1–2**. By this mean, both coumarin nucleus and phenyl unit facilitate radical reactions. The E_{HOMO} and E_{LUMO}, as well as the E_{gap} (band gap energy) $= E_L - E_H$ are significant elements used to describe antioxidative activity. A molecule with a higher E_{HOMO} value is an excellent electron donor and has the best antioxidative activity [17]. The E_{HOMO} values of compound **1** range from −7.159 to −7.055 eV, and are higher than those of compound **2** (−7.525 to −7.422 eV) (Fig. 4). In addition, the E_{gap} values of 5.848–5.872 eV assigning to compound **1** are always lower than those of compound **2** (E_{gap} = 6.266–6.282 eV). These current findings are in line with the experimental results since compound **1** had an antioxidative effect better than compound **2**.

Spin density reflects the speed of free radical quenching reaction. The more delocalization of spin density mainly causes the easier radical formation and the faster reaction speed [18]. The gaseous spin densities of studied compounds **1–2** at the M06-2X/6–311++g(d,p) level, with the visual results using Gaussview 6.0 software, are shown in Fig. 5. The spin density generally evenly distributes in whole aromatic rings of two compounds. For instance, **1**–3′-O-radical contains negative charges at carbons C-1′, C-3′, and C-5′, whereas positive charges are found to locate at carbons C-2′, C-4′, and C-4′. It suggests that aromatic rings provide a good condition for radical formations. Importantly, the BDE and spin density are intimately correlated, which the lower spin density results in a lower BDE [18]. **1**–4′-O• radical contains the lowest spin density of 0.314, as well as each O•-radical in compound **1** has a lower spin density than the correspondence O•-radical in compound **2**. Therefore, it is expected that **1**–4′-OH will have the lowest gaseous BDE, and each hydroxy group of **1** induces a lower BDE than the correspondence hydroxy group of **2**.

NBO (natural bond orbital) analysis

Electron delocalization from a donor (occupied Lewis type) to an acceptor (unoccupied non-Lewis type) in compounds **1–2** was taken into consideration by NBO analysis at the same DFT-B3LYP/6–311++G(d,p) level. Followed by the second-order perturbation theory, the stabilization $E^{(2)}$ energy is deduced from conjugation and hyper-conjugation interactions, and electron density transfer between donor and acceptor, as shown in Eq. (7) [13].

$$E^{(2)} = X_{ij} = q^{i}\left(Y_{ij}\right)^{2}/(X_{j} - X_{i}) \tag{7}$$

where q^i and Y_{ij} stand for the orbital occupancy, and the off-diagonal NBO Fock matrix element, respectively. X_i and X_j stand for diagonal elements. By means of this, the higher $E^{(2)}$ will correspond to the more interaction and the more electron donation. Regarding compound **1**, its ring A is stabilized by various conjugation interactions, including π(C5 – C6) → π*(C4a – C8a) and π*(C7 – C8), π(C4a – C8a) → π*(C5 – C6) and π*(C7 – C8),

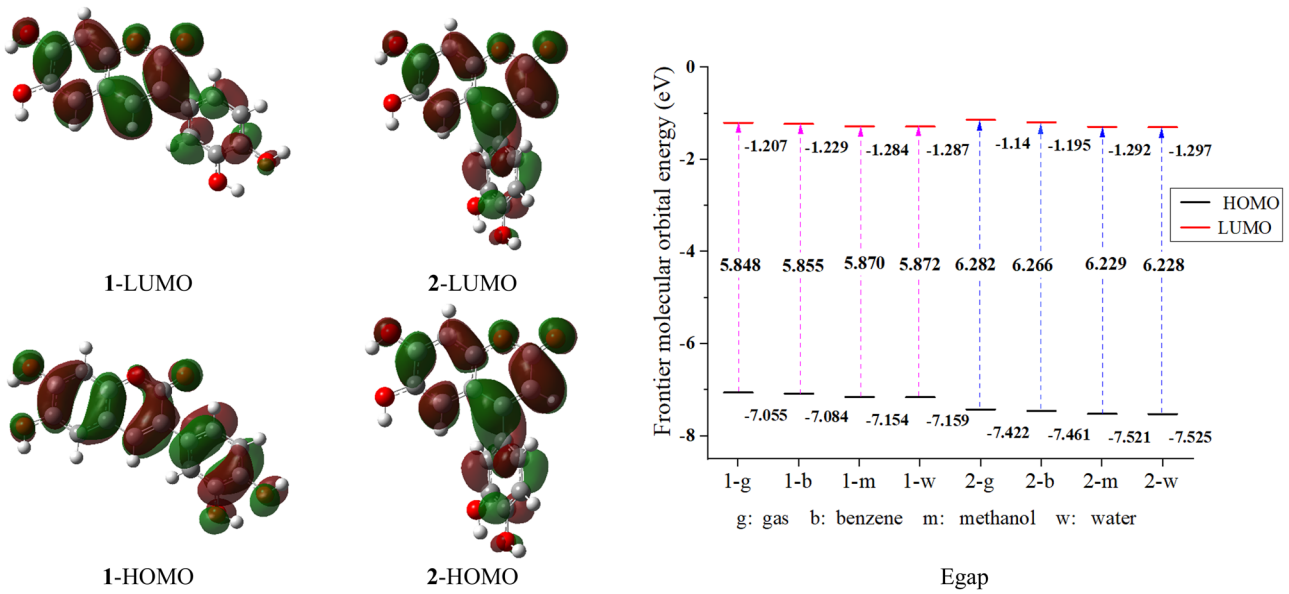

Fig. 4 HOMO and LUMO images and $E_{gap} = E_L - E_H$ of neutral structures **1–2** in both four studied mediums

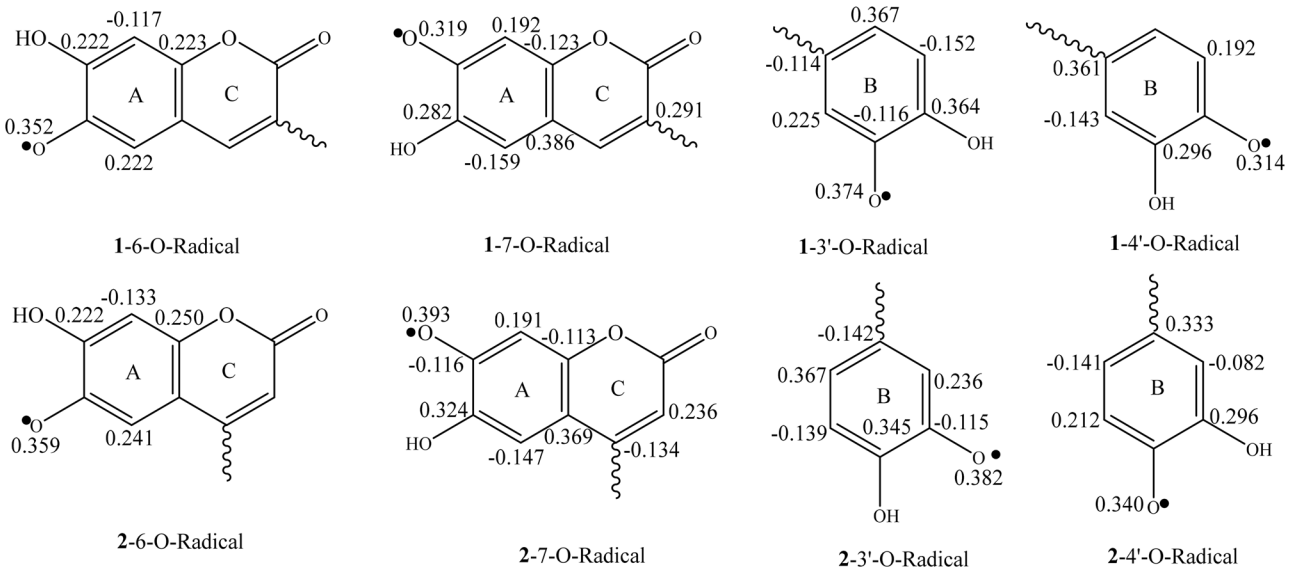

Fig. 5 The selective spin densities of studied compounds **1–2** at the M06-2X/6–311++G(d,p) level

π(C7 – C8) → π*(C4a – C8a) and π*(C5 – C6), LP(2) C6 – O → π*(C5 – C6), and LP(2)C7 – O → π*(C7 – C8) (Table S3). Similarly, ring C is associated with various conjugation interactions such as π(C4a – C8a) → π*(C3 – C4), π(C3 – C4) → π*(C2 = O), LP(2)C2 = O → σ*(C2 = O), π*(C2 = O), and π*(C4a – C8a). Phenyl ring B is characterized by π(C1′ – C6′) → π*(C2′ – C3′), π(C2′ – C3′) → π*(C1′ – C6′), π(C4′ – C5′) → π*(C1′ – C6′), π*(C2′ – C3′), and LP(2)C3′ – O → π*(C2′ – C3′). The $E^{(2)}$ energy of this coumarin ranges from 8.60 to 45.55 kcal/mol. Of compound **2**, two typical interactions σ → σ* and LP (lone pair) → σ* are prevalent (Table S3). For instance, hyper-conjugation σ(C2′ – C3′) → σ*(O′3-H) produces the highest $E^{(2)}$ value of 3353.45 kcal/mol, or LP(2)O1 → σ*(C4 – C4a) gives the significant $E^{(2)}$ value of 3089.45 kcal/mol. Collectively, it can be pronounced that lone pair electrons in oxygen atoms of aromatic compounds are one of the main causes for change of charge distribution, directly affecting to radical reactions [19].

Antioxidative activity

HAT mechanism

Apparently, bond breaking in the HAT mechanism is due to hemolytic cleavage. This process is generally explained by the BDE. The reaction BDE values of compounds **1–2** were calculated at the M06-2X/6–311++g(d,p) level. Regarding compound **1**, in agreement with the spin density, the lowest and highest BDE values of 76.8 and 86.2 kcal/mol were assigned to **1**–4′-OH and **1**–3′-OH in the gaseous phase, respectively (Table 1). In each medium, the BDE values of **1**–6-OH and **1**–4′-OH are always lower than those of **1**–7-OH and **1**–3′-OH. In contrast to **1**–6-OH and **1**–4′-OH, the BDE values of **1**–7-OH and **1**–3′-OH tend to increase when converted gas into solvents. Compound **2** has the lowest and highest BDE values of 77.7 and 88.0 kcal/mol at **2**–6-OH and **2**–3′-OH, respectively. Similar to compound **1**, the BDE values of **2**–6-OH and **2**–4′-OH are always lower than those of **2**–7-OH and **2**–3′-OH. Additionally, the BDE value in each correspondence OH group of compound **1** is always lower than that of compound **2**. Hence, it is possibly concluded that the antioxidative activity of **1** is better than **2**, and this is well agreed with the experimental result [5].

SET-PT and SPL-ET mechanisms

The first step of SET-PT is characterized by the IP calculation. As shown in Table 1, the IP values of both two compounds is much dependent on the change of environment, and they are found to run in an order of gas > benzene >> methanol > water. It can be concluded that the electron loss from M-OH to form radical cation M-OH$^{\bullet+}$ will be better in polar mediums. The second step of SET-PT is a heterolytic process and is monitored by the PDE. It is found that the gaseous PDE values of two compounds **1–2** are much greater than those in solvents, and an order for both two compounds is gas >> benzene > water > methanol. It reflects that the medium polar, like alcoholic methanol, would help to reduce the PDE energy. This phenomenon is also detected in phenolic compounds [19, 20]. Hydroxy groups at C-6 and C-4′ of both two compounds have the lowest PDE values in methanol. Similar

Table 1 Studied phases reaction enthalpies at 298 K for radicals of compounds **1–2** at the M06-2X/6–311++G(d,p) level (in kcal/mol)

No	BDE				IP				PDE			
	Gas	Benzene	MeOH	Water	Gas	Benzene	MeOH	Water	Gas	Benzene	MeOH	Water
1–6-OH	77.2	78.1	79.5	79.5	172.1	151.4	119.1	114.0	219.9	26.2	6.6	11.1
1–7-OH	85.7	84.6	83.1	83.0					228.4	32.7	10.2	14.5
1–3′-OH	86.2	84.8	83.2	83.1					228.9	32.9	10.3	14.6
1–4′-OH	76.8	77.1	77.8	77.8					219.5	25.3	4.9	9.3
2–6-OH	77.7	78.6	79.8	79.9	182.6	160.1	125.5	120.2	210.0	18.0	0.6	5.2
2–7-OH	87.3	86.3	84.8	84.7					219.6	33.6	5.5	10.0
2–3′-OH	88.0	86.7	84.7	84.6					220.3	34.0	5.4	9.8
2–4′-OH	79.0	79.6	80.2	80.2					211.3	26.9	0.9	5.5

No	PA				ETE			
	Gas	Benzene	MeOH	Water	Gas	Benzene	MeOH	Water
1–6-OH	323.6	88.4	37.4	40.5	68.5	89.2	88.3	84.5
1–7-OH	329.2	92.8	39.1	42.4	71.3	91.3	90.2	86.5
1–3′-OH	345.0	104.8	47.1	49.8	56.0	79.5	82.3	78.8
1–4′-OH	328.0	92.2	39.4	42.0	63.6	84.6	84.6	80.9
2–6-OH	325.8	89.7	37.8	40.8	66.8	88.4	88.3	84.6
2–7-OH	331.7	93.9	39.2	42.0	70.5	91.9	91.9	88.2
2–3′-OH	336.7	99.6	45.3	48.1	66.2	86.6	85.6	81.9
2–4′-OH	320.9	87.1	37.5	40.4	72.9	92.0	89.2	85.3

to the BDE, the PDE values of 6-OH and 4′-OH of both two compounds are lower than those of 7-OH and 3′-OH in each medium (Table 1). However, in contrast to the BDE, the PDE value in each correspondence OH group of compound **2** is lower than that of compound **1** in each correspondence medium.

The deprotonation to produce anion M–O$^-$ in the SPL-ET mechanism is monitored by the PA. From Table 1, the lowest PA values belong to **1**–6-OH (37.4 kcal/mol), **1**–4′-OH (39.4 kcal/mol), **2**–6-OH (37.8 kcal/mol), and **2**–4′-OH (37.5 kcal/mol) in methanol. It resembles the PDE, the PA values of both two compounds **1–2** are orderly run as gas >> benzene > water > methanol. In each medium, 6-OH and 4′-OH in each compound induced the lower PA values than those of 7-OH and 3′-OH. The ETE energy represents electron transfer in the second step of the SPL-ET mechanism. Hydroxy groups at carbons C-3′ of two studied compounds **1–2** exert the lowest gaseous ETE values of 56.0 and 66.2 kcal/mol, respectively, whereas the highest ones are assigned to **1**–7-OH (91.3 kcal/mol), and **2–**4′-OH (92.0 kcal/mol). In each medium, 3′-OH of each compound possesses the ETE value lower than that of the remaining OH groups. In each OH case, the gaseous ETE value is always lower than that in solvents. It is argued that non-polar medium, like the gaseous phase, is appropriate for electron transfer. Taken together, similar to the previous result [9], it can be concluded that the antioxidative actions of phenylcoumarins were deduced from O**–**H bond cleavages.

Favorable mechanism

The preferential antioxidative mechanism for compounds **1–2** is generally decided by the lowest BDE, IP, and PA enthalpies [20–22]. Obviously, the PA values in methanol and water are lower than the BDE and IP values. As a consequence, the SPL-ET mechanism is essential for both two studied compounds **1–2** in polar solvents. However, considering gas and benzene, it is viewed that the BDE values are less than the IP and PA values. Hence, the HAT seems to be the appropriate mechanism in weak or non-polar mediums.

Kinetic study

Apparently, the ROS agents, such as HOO$^\bullet$, have induced harmful oxidative processes and mainly caused serious illnesses such as cancer, kidney injury, atherosclerosis, and heart failure [23]. In this section, we then proposed a kinetic model by the interaction between compounds **1–2** and HOO$^\bullet$. The calculation was performed in the gaseous phase at the same theoretical M06-2X/6–311++G(d,p) level, and the results are shown in Table 2 and Figs. 6 and S1. The rate constant K and the Gibbs free energy of activation $\Delta G^{\#}$ are two key elements to evaluate a kinetic reaction, by which a good reaction site will have the lowest K and $\Delta G^{\#}$ values [24]. The obtained result agrees with the above enthalpy calculation, in which **1**–6-OH and **1**–4′-OH possess the lowest $\Delta G^{\#}$ values of 12.3 and 12.9 kcal/mol, and the lowest K

Table 2 The gaseous $\Delta G^{\#}$ and *k* for HOO$^{\bullet}$ and $^{\bullet}NO_2$ radical attacks at the M06-2X/6–311++G(d,p) level and 298.15 K

Reaction	$\Delta G^{\#}$ (kcal/mol)	*K* (L/mol.s)	Reaction	$\Delta G^{\#}$ (kcal/mol)	*K* (L/mol.s)
Compounds **1–2** + HOO$^{\bullet}$ radical					
1-6-OH	12.3	1.27×10^{4}	**2**–6-OH	13.2	3.95×10^{3}
1–7-OH	14.1	4.03×10^{2}	**2**–7-OH	23.4	7.43×10^{-2}
1–3′-OH	21.9	1.45×10^{-1}	**2**–3′-OH	22.4	7.30×10^{-2}
1–4′-OH	12.9	5.03×10^{3}	**2**–4′-OH	14.1	1.53×10^{3}
Compounds **1–2** + $^{\bullet}NO_2$ radical					
1–6-OH	19.1	5.80	**2**–6-OH	18.4	1.29×10^{1}
1–7-OH	20.4	9.37×10^{-1}	**2**–7-OH	25.1	4.42×10^{-4}
1–3′-OH	22.6	3.40×10^{-2}	**2**–3′-OH	25.5	2.69×10^{-4}
1–4′-OH	19.1	3.41	**2**–4′-OH	22.0	1.14×10^{-1}

values of 5.03×10^{3} and 1.27×10^{4} L/mol s, respectively. **1**–3′-OH exhibits the highest $\Delta G^{\#}$ value of 21.9 kcal/mol, and the lowest *K* value of 1.45×10^{-1} L/mol s. In the same manner, hydroxyl groups at C-6 and C-4′ of compound **2** have induced the lowest $\Delta G^{\#}$ values of 13.2–14.1 kcal/mol, and the lowest *K* values of 1.53–3.95 10^{3} L/mol s, while hydroxyl groups at C-7 and C-3′ are opposite. The $\Delta G^{\#}$ and *K* values of each hydroxy group in compound **1** are always better than those of the correspondence group in compound **2** (Table 2). It is also found that the relative energy of transition state (TS) of each hydroxy group in compound **1** is always better than that of the correspondence group in compound **2** (Fig. 6).

The current study also deals with another interaction between compounds **1–2** and the representative RNS radical $^{\bullet}NO_2$. From Fig. S2, the reactions of each hydroxy group and $^{\bullet}NO_2$ have undergone one transition state and one intermediate. In each compound, hydroxy groups at carbons C-6 and C-4′ generate the lowest $\Delta G^{\#}$ and *K* values, and are better than those of C-7 and C-3′ (Table 2). Once again, the $\Delta G^{\#}$, *K*, and TS relative energy of each hydroxy group in compound **1** are found better than those of the correspondence group in compound **2** (Table 2 and Fig. 7). With the better $\Delta G^{\#}$ and *K* values, compounds **1–2** have faster kinetic reaction with HOO$^{\bullet}$ radicals than with $^{\bullet}NO_2$ radicals.

Acidic assessment

The acidity of a molecule is referred to as the deprotonated capacity [6, 25–27]. Therefore, the acidic consideration is a good way to evaluate antioxidative activity, as well as two parameters pKa and $\Delta H_{acidity}$ are two popular concepts [25–27].

The pK_a values were collected from the thermodynamic diagram (Fig. 8) and Eqs. (8)–(10).

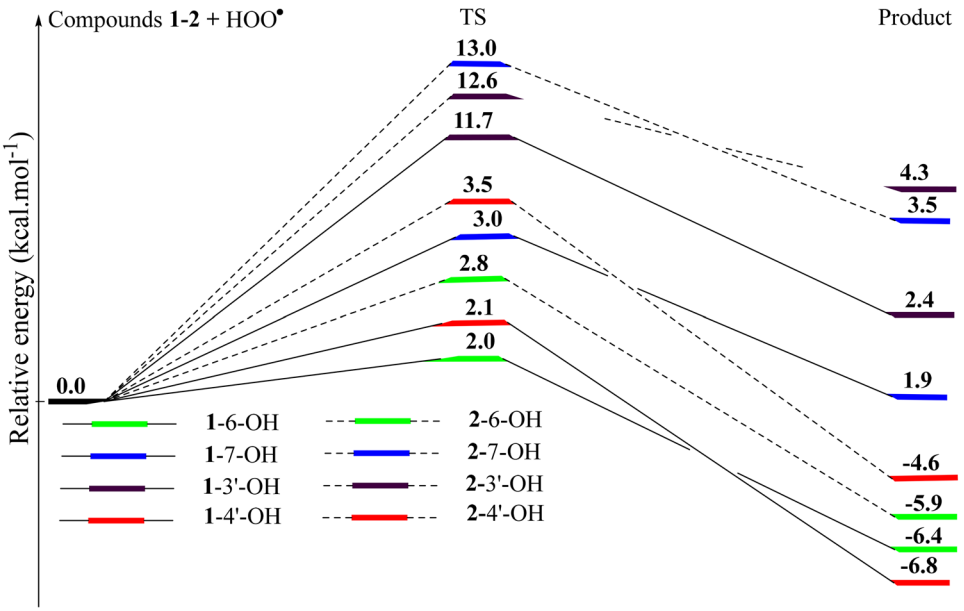

Fig. 6 Energy diagram for the reaction of HOO$^{\bullet}$ radical attack to compounds **1**–**2** at the M06-2X/6–311++G(d,p) level

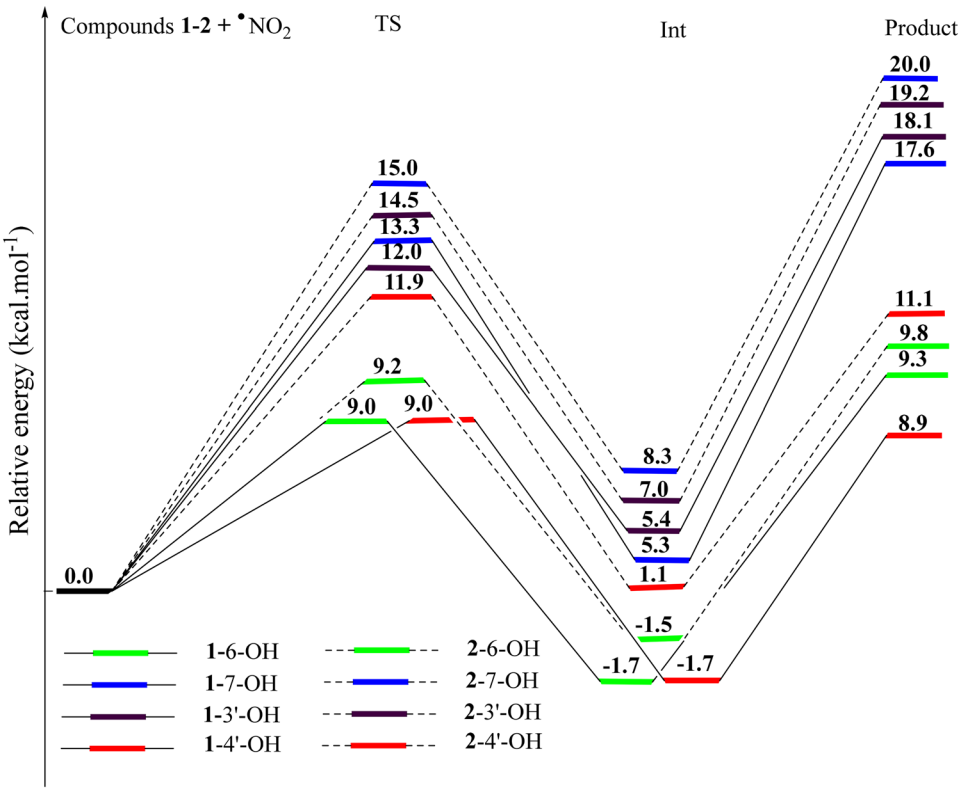

Fig. 7 Energy diagram for the reaction of $^{\bullet}NO_2$ radical attack to compounds **1**–**2** at the M06-2X/6-311G(d,p) level

$$\Delta G_{sol} = \Delta G_g + \Delta G_{sol}(M-O^-) + \Delta G_{sol}(H_3O^+) - \Delta G_{sol}(M-OH) - \Delta G_{sol}(H_2O) \quad (8)$$

$$pK_a = \Delta G_{sol}/1.364 - \log[H_2O] \quad (9)$$

$$pK_a, \text{ corrected} = pK_a, \text{ calculated} - 4.54 \quad (10)$$

where the ΔG_{sol} values for H_2O (−6.31 kcal/mol) and H_3O^+ (−110.2 kcal/mol) were collected from experiments [25–27].

The aqueous $\Delta H_{acidity}$, which is equal to E(M–O$^-$) − E(M-OH), is calculated at 298 K.

From Table S3, **1**–6-OH exerts the lowest $pK_{a,\text{ corrected}}$ value of 8.65 and the lowest $\Delta H_{acidity}$ value of 322.08 kcal/mol, while the highest $pK_{a,\text{ corrected}}$ value of 15.49 and the highest $\Delta H_{acidity}$ value of 343.53 kcal/mol belong to **1**–3′-OH. In the meantime, **2**–4′-OH generates the lowest $pK_{a,\text{ corrected}}$ and $\Delta H_{acidity}$, and **2**–3′-OH gives the highest ones (Table S3). These results make a good agreement with the aqueous PA values. It is worth that **1**–6-OH and **2**–4′-OH are good sites for deprotonation.

Metal complex chelation

Another antioxidative feature of natural product compounds is their interaction with metal ions, which resulted in complexes that suppressed the participation of metal ions in free radical-producing processes [28].

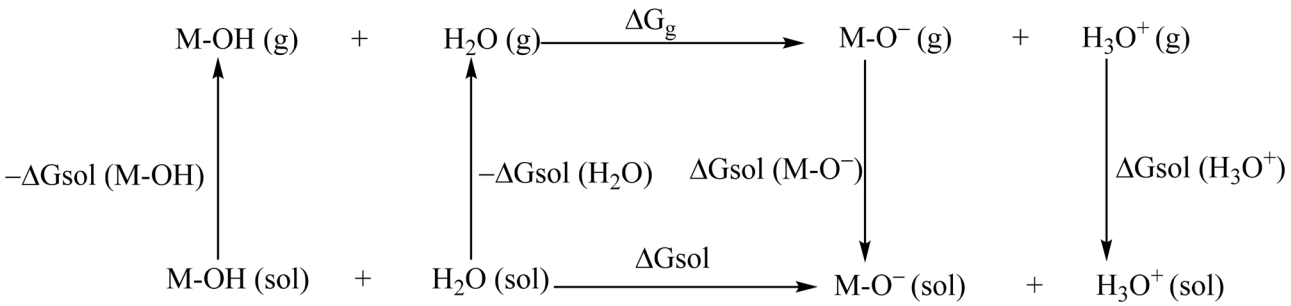

Fig. 8 Acid dissociation diagram of the studied compounds **1–2**

In this section, we deal with a possible complex model [Fe(coumarin)$_2$(H_2O)$_2$] when chelated between two studied compounds **1–2** and Fe^{2+} in methanol, including complex **I** (**1**–6-OH and **1**–7-OH + Fe^{2+}), complex **II** (**1**–3′-OH and **1**–4′-OH + Fe^{2+}), complex **III** (**2**–6-OH and **2**–7-OH + Fe^{2+}), and complex **IV** (**2**–3′-OH and **2**–4′-OH + Fe^{2+}) (Table 3 and Figs. 9 and S3). As far as we know, the iron ion is now popular in antioxidative experiments type metal chelation, as well as the M06-2X/6-311G(d,p)/LANL2DZ level has been often selected for metal chelation calculations [29–31]. The optimized processes and the calculations of interaction energy (IE) and metal interaction analysis (MIA) of these complexes **I–IV** were performed in methanol at the M06-2X/6-311G(d,p)/LANL2DZ level. The TD-DFT/M06-2X/6-311G(d,p)/LANL2DZ method was used to view the UV–Vis data.

Two descriptors IE and MIA indicate the stability of metal–ligand interactions [32]. The IE is ruled by a BSSE (basis set superposition error) correction (Eq. (11)).

$$IE_{MN} = E_{MN} - (E_M + E_N) \quad (11)$$

where E_{MN}, E_M, and E_N are energies of complex MN, and single compounds M and N, respectively.

The MIA is a negative sign of ΔH^0_{298} (Eq. (12))

$$MIA = -\Delta H^0_{298} = -[H^0_{298,AB} - (H^0_{298,A} + H^0_{298,B})] \quad (12)$$

Generally, the optimized complexes I–IV were obtained in octahedral symmetric forms (Fig. S3). The IE values are arranged as complex **II** (−189.6 kcal/mol) < IV (−186.5 kcal/mol) < **III** (−186.1 kcal/mol) < **I** (−186.0 kcal/mol), whereas the MIA are obtained as complex **II** (284.7 kcal/mol) > **IV** (283.0 kcal/mol) > **III** (282.8 kcal/mol) > **I** (282.3 kcal/mol) (Fig. 9). It concludes that complex **II** is the most stable, as well as complexes I and III are unstable forms.

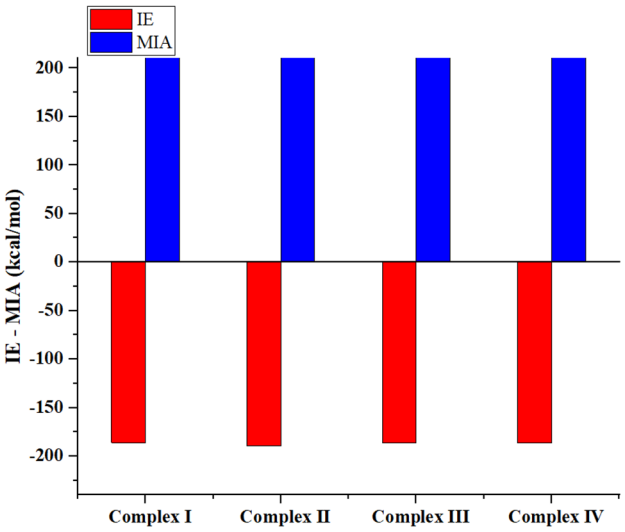

Fig. 9 The IE and MIA (kcal/mol) for complexes **I–IV** at the theoretical M06-2X/6-311G(d,p)/LANL2DZ level

To date, the UV–Vis data of compounds **1–2** are not available. By the TD-DFT/M06-2X/6–311++G(d,p) method, two λ_{max} of compound **1** have peaked at 194 nm [E_{vert} = 6.405 eV, f = 0.316, and HOMO-2 → LUMO + 8 (23%)], and 323 nm [E_{vert} = 3.842 eV, f = 0.747, and HOMO → LUMO (94%)], while two peaks of compound **2** located at 195 nm [E_{vert} = 6.362 eV, f = 0.219, and HOMO → LUMO + 5 (12%)], and 303 nm [E_{vert} = 4.091 eV, f = 0.340, and HOMO → LUMO (91%)] (Table 3). As compared to compounds **1–2**, the λ_{max} values tend to the long wavelengths. For instance, the stable complex **II** contains the first band [λ_{max} = 255 nm, E_{vert} = 4.858 eV, f = 0.081, and HOMO-7 → LUMO (19%)], and the second band [λ_{max} = 353, E_{vert} = 3.509 eV,

Table 3 The UV–Vis of compounds **1–2** and their complexes **I–IV** in methanol: calculated at the M06-2X/6-311G(d,p) level for compounds **1–2** and at the M06-2X/6-311G(d,p)/LANL2DZ level for complexes **I–IV**

No	λ_{max} (nm)	E_{vert} (eV)	f	Excitation transition
Compound **1**	194	6.405	0.316	H − 2 → L + 8 (23%)
	323	3.842	0.747	H → L (94%)
Compound **2**	195	6.362	0.219	H → L + 5 (12%)
	303	4.091	0.340	H → L (91%)
Complex **I** (**1**–6-OH and **1**–7-OH + Fe^{2+})	295	4.199	0.780	H − 2 → L (42%)
	349	3.550	0.866	H → L (44%)
Complex **II** (**1**–3′-OH and **1**–4′-OH + Fe^{2+})	255	4.858	0.081	H − 7 → L (19%)
	353	3.509	1.518	H → L (29%)
Complex **III** (**1**–6-OH and **1**–7-OH + Fe^{2+})	257	4.817	0.486	H → L + 4 (27%)
	345	3.595	0.410	H → L (41%)
Complex **IV** (**2**–3′-OH and **2**–4′-OH + Fe^{2+})	240	5.160	0.183	H → L + 4 (33%)
	330	3.761	0.883	H → L (38%)

E_{vert} vertical transition energy, f oscillator strength

$f = 1.518$, and HOMO → LUMO (29%)]. Herein, new information on the physicochemical features of complexes between Fe^{2+} with compounds **1–2** is provided.

Conclusion

For the first time, the DFT calculation in the current work effectively provides detailed information on the antioxidative activity of the two studied coumarins **1–2**. In the light of structural and electronic analyses, the cleavage of OH bond mainly causes free radical quenching. At the M06-2X/6–311++G(d,p) level, the HAT mechanism is preferential for compounds **1–2** in gas and benzene, but the SPL-ET mechanism is appropriate in polar solvents methanol and water. Hydroxy groups at C-6 and C-4′ of both two compounds are good sites for antiradical since they had the lowest BDE values of 76.8–79.6 kcal/mol in gas and benzene, and the lowest PA values of 37.4–40.8 kcal/mol in methanol and water. It is also viewed that hydroxy groups at C-6 and C-4′ of both two compounds are better than hydroxyl groups at C-7 and C-3′ in the kinetic reactions with $HOO^{\bullet}$ and $^{\bullet}NO_2$ radicals. **1**–6-OH shows the best acidity (deprotonation) with the lowest $pK_{a,\ corrected}$ value of 8.65 and the lowest $\Delta H_{acidity}$ value of 322.08 kcal/mol. Two *ortho* hydroxy groups of phenyl ring in compound **1** have chelated to Fe^{2+}, to form the most stable complex with the lowest IE value of −189.6 kcal/mol, and the highest MIA value of 284.7 kcal/mol. It is consistent with the experimental results, the current computational result confirms that coumarin **1** is better than coumarin **2** for antioxidative purposes.

Abbreviations BDE: Bond dissociation energy; DFT: Density functional theory; E_{gap}: Band gap energy; FMO: Frontier molecular orbital; HAT: Hydrogen atom transfer; HOMO: Highest occupied molecular orbital; IE: Interaction energy; IP: Ionization potential; LUMO: Lowest unoccupied molecular orbital; MIA: Metal interaction analysis; NBO: Natural bond orbital; PA: Proton affinity; PDE: Proton dissociation enthalpy; SET-PT: Single electron transfer-proton transfer; SPL-ET: Sequential proton loss-electron transfer; TST: Transition state theory; $\Delta G^{\#}$: Gibbs free energy of activation

Supplementary Information The online version contains supplementary material available at https://doi.org/10.1007/s11224-023-02183-3.

Author contribution P. T. T. contributed to the conception of the study; D. X. D. performed the data analyses; N. T. S. wrote the manuscript. All authors read and approved the final manuscript.

Data availability The data used and/or analyzed during the current study are available from the corresponding author on reasonable request.

Declarations

Ethics approval This article does not contain any studies involving animals performed by any of the authors.

Consent to participate This article does not contain any studies involving animals performed by any of the authors.

Consent for publication The author mentioned in the manuscript has given consent for submission and subsequent publication of the manuscript.

Conflict of interest The authors declare no competing interests.

References

1. Detsi A, Kontogiorgis C, Hadjipavlou-Litina D (2017) Coumarin derivatives: an updated patent review (2015–2016). Expert Opin Ther Pat 27:1201–1226
2. Srikrishna D, Godugu C, Dubey PK (2018) A review on pharmacological properties of coumarins. Mini-Rev Med Chem 18:113–141
3. Paya M, Halliwell B, Hoult JRS (1992) Interactions of a series of coumarins with reactive oxygen species: scavenging of superoxide, hypochlorous acid and hydroxyl radicals. Biochem Pharmacol 44:205–214
4. Jung Y, Jung J, Huh Y, Kim D (2018) Benzo[g]coumarin-based fluorescent probes for bioimaging applications. J Anal Method Chem 5249765
5. Danis O, Demir S, Gunduz C, Alparslan AM, Altun S, Yuce-Dursun BY (2016) Synthesis of selected 3- and 4-arylcoumarin derivatives and evaluation as potent antioxidants. Res Chem Intermed 42:6061–6077
6. Mardirossian N, Gordon MH (2017) Thirty years of density functional theory in computational chemistry: an overview and extensive assessment of 200 density functionals. Mol Phys 115:2315–2372
7. Mardirossian N, Gordon MH (2016) How accurate are the Minnesota density functionals for noncovalent interactions, isomerization energies, thermochemistry, and barrier heights involving molecules composed of main-group elements? J Chem Theory Comput 12:4303–4325
8. Goerigk L, Hansen A, Bauer C, Ehrlich S, Najibi A, Grimme S (2017) A look at the density functional theory zoo with the advanced GMTKN55 database for general main group thermochemistry, kinetics and noncovalent interactions. Phys Chem Chem Phys 19:32184
9. Karadjova V, Popovska MV, Velkov Z (2021) Radical-scavenging activity characterization of a series of synthetic 3-phenylcoumarins. Comput Theore Chem 1202:113300
10. Souza GLCD, Peterson KA (2021) Benchmarking antioxidant-related properties for gallic acid through the use of DFT, MP2, CCSD, and CCSD(T) approaches. J Phys Chem A 125:198–208
11. Thuy PT, Son NT (2022) Thermodynamic and kinetic studies on antioxidant capacity of amentoflavone: a DFT (density functional theory) computational approach. Free Rad Res 56:526–525
12. Zhao Y, Truhlar DG (2008) How well can new-generation density functionals describe the energetics of bond-dissociation reactions producing radicals? J Phys Chem A 112:1095–1099
13. Yadav AK, Mishra BK, Singh A, Gour NK (2022) Atmospheric degradation, mechanism and kinetics of ethyl vinyl ketone (CH_2=$CHCOCH_2CH_3$) initiated by Cl atom: an insight from DFT study. Mol Phys 120:e2100835
14. Thuy PT, Trang NV, Duc DX, Son NT (2021) The antioxidative potential of benzofuran-stilbene hybrid derivatives: a comparison between natural and synthetic compounds. Struct Chem 32:2271–2281
15. Klein E, Lukes V (2007) DFT/B3LYP study of the substituent effect on the reaction enthalpies of the individual steps of

sequential proton loss electron transfer mechanism of phenols antioxidant action: Correlation with phenolic C-O bond length. J Mol Struct Theochem 805:153–160
16. Boulebd H (2019) DFT study of the antiradical properties of some aromatic compounds derived from antioxidant essential oils: C-H bond vs. O–H bond. Free Rad Res 53:1125–1134
17. Reza Nazifi SM, Asgharhamsi MH, Dehkordi MM (2019) Antioxidant properties of *Aloe vera* components: a DFT theoretical evaluation. Free Rad Res 53:922–931
18. Saqib M, Iqbal S, Mahmood A, Akram R (2016) Theoretical investigation for exploring the antioxidant potential of chlorogenic acid: a density functional theory study. Int J Food Prop 19:745–751
19. Son NT, Thuy PT, Trang NV (2021) Antioxidative capacities of stilbenoid Suaveolensone A and Flavonoid Suaveolensone B: a detailed analysis of structural-electronic properties and mechanisms. J Mol Struct 1224:129025
20. Thuy PT, Son NT (2021) Thermodynamic study on antioxidative action of cynandione A: a DFT approach. Struct Chem 32:1807–1817
21. Amic D, Stepanic V, Lucic B, Markovic Z, Markovic JMD (2013) PM6 study of free radical scavenging mechanisms of flavonoids: why does O-H bond dissociation enthalpy effectively represent free radical scavenging activity? J Mol Model 19:2593–2603
22. Xue Y, Zheng Y, Zhang L, Wu W, Yu D, Liu Y (2013) Theoretical study on the antioxidant properties of 2′-hydroxychalcones: H-atom vs. electron transfer mechanism. J Mol Model 19:3851–3862
23. Kaur C, Kapoor HC (2001) Antioxidants in fruits and vegetables – the millennium's health. Int J Food Sci Technol 36:703–725
24. Trang NV, Thuy PT, Thanh DTM, Son NT (2021) Benzofuran–stilbene hybrid compounds: an antioxidant assessment – a DFT study. RSC Adv 21:12971–12980
25. Boulmokh Y, Belguidoum K, Meddour F, Amira-Guebailia H (2021) Investigation of antioxidant activity of epigallocatechin gallate and epicatechin as compared to resveratrol and ascorbic acid: experimental and theoretical insights. Struct Chem 32:1907–1923
26. Charif IE, Mekelleche SM, Villemin D, Mora-Diez N (2007) Correlation of aqueous pK_a values of carbon acids with theoretical descriptors: A DFT study. J Mol Struct 818:1–6
27. Ali ST, Choudhary A, Khalil SM, Arif Z (2021) A simple computational approach for pKa calculation of organosulfur compounds. J Serb Chem Soc 86:165–170
28. Fernandez MT, Mira ML, Florencio MH, Jennings KR (2002) Iron and copper chelation by flavonoids: an electrospray mass spectrometry study. J Inorg Biochem 92:105–111
29. Kim HJ, Chen F, Wang X, Chung HY, Jin Z (2005) Evaluation of antioxidant activity of Vetiver (*Vetiveria zizanioides* L.) oil and identification of its antioxidant constituents. J Agric Food Chem 53:7691–7695
30. Gholivan K, Gholami A, Schenk KJ, Erafili MD, Farshadfar K (2015) Supramolecular assemblies of organotin(IV)–diphosphoryl adducts: insights from X-rays and DFT. RSC Adv 5:98610–98617
31. Patil M (2016) Mechanistic insights into the initiation step of the base promoted direct C-H arylation of benzene in the presence of additive. J Org Chem 81:632–639
32. Shankar R, Kolandaivel P, Senthilkumar L (2011) Interaction studies of cysteine with Li^+, Na^+, K^+, Be^{2+}, Mg^{2+}, and Ca^{2+} metal cation complexes. J Phys Org Chem 24:553–567